ELSEVIER

Journal of Power Sources 58 (1996) 197–203

JOURNAL OF POWER SOURCES

Short Communication

Electrochemical corrosion of an Al–Mg–Cr–Mn alloy containing Fe and Si in inhibited alkaline solutions

A.M.M.M. Adam, N. Borràs, E. Pérez, P.L. Cabot *

Departament de Química Física, Facultat de Química, Universitad de Barcelona, Martí Franquès 1, 08028 Barcelona, Spain

Received 17 May 1995; revised 24 January 1996; accepted 9 February 1996

Abstract

The electrochemical corrosion of Al–2.7%Mg–0.19%Cr–0.04%Mn alloy containing 0.27% Fe and 0.14% Si, using open-circuit potential measurements, corrosion rate determinations, potentiodynamic and galvanostatic transients and anode efficiency experiments together with optical microscopy, scanning electron microscopy, transmission electron microscopy and energy dispersion X-ray has been studied to ascertain the effect of Cr and Mn. The experiments were performed at 25 and 50 °C in non-deaerated and stirred 4 M KOH containing K_2MnO_4 and combinations of $NaVO_3$, $NaBiO_3$, $NaMoO_4$, ZnO and Al_2O_3. The open-circuit potentials were rapidly stabilized in values in the range between −1.4 and −1.6 V versus Hg/HgO/OH^- (4 M KOH). The alloy dissolution at open circuit and also in the galvanostatic and potentiodynamic experiments were shown to be uniform, this being correlated with the homogeneous distribution of Mg in the material. The anodic oxidation took place with the formation and dissolution of a conducting aluminium oxide film. However, limiting values were found over which the anode became passivated. The limiting values depended on the temperature, being about 125 and 500 mA cm^{-2} at 25 and 50 °C, respectively. The anode efficiencies were sufficiently high, that is over 90%, only at current densities approaching the limiting value at the corresponding temperature. The anode passivation was related to an excess of Cr and the anode corrosion to an excess of Mg together with the presence of Fe and Si.

Keywords: Corrosion; Aluminium; Magnesium; Chromium; Manganese; Iron; Silicon; Alkaline solution

1. Introduction

Aluminium and aluminium alloys are theoretically very good fuels for electrical power sources [1–5], the Al/air device in alkaline solutions being the highest energy density system amongst those able to replace internal combustion engines for vehicles. In practice, they may suffer significant parasitic corrosion, anode polarization or poor performance. However, the Al/air battery is still recognized to be sufficiently attractive and a significant effort is currently being performed to solve these limitations. Even in the case that H_2 evolution produced in the parasitic corrosion could never be eliminated, the electrolyte removal from the anode when the cell does not operate [6] and the attempt to use this H_2 in a H_2/O_2 fuel cell [7] have been foreseen.

The corrosion rate of super-pure aluminium in alkaline solutions depends on the electrolyte nature, concentration and temperature [8–10]. In order to decrease the parasitic corrosion, the behaviour of super-pure aluminium in alkaline solutions with the addition of organic and inorganic inhibitors has been explored in the past [11–16]. The general result was that the anode efficiencies were greater in the presence of inorganic inhibitors such as K_2CrO_4 and $(NH_4)_2MoO_4$.

Another approach to the Al/air batteries performance consists of small additions to super-pure Al of alloying elements such as gallium, indium and thallium, metals which considerably shift the open-circuit potential to the negative direction [17,18]. A special attention has been given to the alloys Al–1%Mg–0.1%In–0.2%Mn (alloy BDW) [19] and to Al–Mg(0.01–5%)–Sn(>0.005%) [20], which present high coulombic efficiencies. A recent approach consists of the addition, to the solution, of compounds derived from those which were useful in the form of alloying elements dissolved in the aluminium anode [2]. Thus, $Ga(OH)_4^-$, $In(OH)_3$ and BiO_3^{3-} together with the oxidant inhibitors SnO_3^{2-} and MnO_4^{2-} were employed for super-pure aluminium in 4 M KOH. However, not all the elements exhibited the same behaviour as when they were dissolved in the metal anode.

On the other hand, studies were made using alloys containing Zn, Mg, In, V, Bi and others based on commercial Al in order to obtain low-cost raw materials [21,22]. Although alloys based on commercial Al generally suffer greater cor-

* Corresponding author.

PII S0378-7753(96)02399-1

rosion rates because of the presence of Fe and Si [23,24], inhibition efficiencies up to 93% at open circuit were reported for commercial Al in a 4 M NaOH solution containing calcium oxide, sodium citrate and zinc oxide.

This work is related to low-cost anodes, that is based on commercial Al which contains Fe and Si. The effect of Mn and Cr on increasing the corrosion resistance of Al is well known [25]. In fact, the positive effect of Mn addition to Al–Mg alloys for alkaline Al batteries has been recently demonstrated [6]. The addition of Mn appears to decrease the potential difference between the matrix and the intermetallics, this reducing the extent of the overall corrosion [26]. The Cr intermetallic compounds are also able to dissolve Fe [25] and probably behave in a similar manner. On the other hand, Mg is a lattice expander which increases the solubility of Fe [27]. According to these ideas, the present work is a first approach to the effect of the addition of Cr and Mn in the anodic behaviour of Al–Mg alloys containing Fe and Si in inhibited and uninhibited alkaline solutions. As a Mn addition over 0.15% produces anode passivation in the Al–0.8%Mg alloys [6], the Mn content has been set at 0.04%. On the other hand, the Mg composition was 2.7% to avoid segregation of Mg intermetallic phases, to counter-balance the shift of the anode potential in the positive direction caused by the Cr addition and also to increase the impurity tolerance of the alloy. These Al–Mg anodes were tested in aerated and vigorously stirred 4 M KOH, at 25 and 50 °C, in the presence and in the absence of Al_2O_3, ZnO, MnO_4^{2-}, BiO_3^-, VO_3^- and MoO_4^{2-}, previously described as efficient inhibitors [1,2,12,21,22], using corrosion potential measurements, potentiodynamic and galvanostatic experiments and optical microscopy, scanning electron microscopy (SEM), transmission electron microscopy (TEM) and energy dispersion X-ray (EDX). The results have been compared with those using super-pure aluminium and commercial grade aluminium.

2. Experimental

2.1. Preparation of the samples

The Al–Mg–Cr–Mn alloy was prepared in liquid state, adding the alloying elements up to the desired composition. Commercial Al and high purity Mg, Cr and Mn were employed to prepare the alloy. The ingot was cooled in water, heated to 350–380 °C, hot-rolled at this temperature and then, cold-rolled to obtain plates having 3 mm in thickness. Any heat treatment was not further performed. The spectrographic analysis of such plates showed 2.7% Mg, 0.19% Cr, 0.04% Mn, 0.27% Fe, 0.14% Si, 0.03% Cu, 0.01% Ti and 0.03% Zn.

From the final alloy plates, disks of 8 mm in diameter were cut (cross section of 0.503 cm^2). The electrical contact was made by a copper wire. Afterwards, the samples were embedded in epoxy resin and encapsulated in a poly(vinyl chloride) (PVC) holder to expose only the base of the alloy disk to the solution.

The results were compared with those obtained using 99.9995% Al and commercial Al. The spectrographic analysis of the latter gave 99.29% Al, 0.39% Fe, 0.2% Si, 0.06% Cu, 0.03% Mn, 0.01% Ti and 0.01% Zn (the Mg content was less than 0.04% and the Cr and Ni contents were each less than 0.01%). The corresponding electrodes were also prepared as disks of 8 mm in diameter, only the base of the disks being polished and exposed to the solution. Before the experiments, the working electrodes were mechanically polished with diamond powder of 1 μm using ethanol in ultrasonic bath to remove the smut.

2.2. Electrochemical tests

All the solutions were prepared using Millipore Milli Q quality water. The reagents were of analytical grade and commercially available (Merck) except K_2MnO_4, which was prepared from $KMnO_4$ [28]. The working electrolytes consisted of a base solution composed of 4 M KOH + 10^{-3} M K_2MnO_4. To this base solution, combinations of 10^{-2} M $NaBiO_3$, 10^{-2} M $NaVO_3$, 10^{-2} M Na_2MoO_4, 0.05% Al (as Al_2O_3) and 0.05% Zn (as ZnO) were added. The experiments were carried out at 25 ± 1 and 50 ± 2 °C in a PVC cell of about 0.5 dm^3 in volume and in stirred solutions. Stirring was performed by a solution jet which entered into the electrolyte at a speed of 28 cm s^{-1} and at a distance of 4 cm from the working electrode (the solution flowed through a PVC pipe using a peristaltic pump).

The auxiliary and reference electrodes were, respectively, a Pt wire and the Hg/HgO/KOH(C), which was connected via a Luggin capillary made of PVC. All the potentials given in this work are referred to this reference electrode.

The open-circuit potential (OCP) versus time as well as the potentiodynamic and the galvanostatic measurements were performed by means of a 273 EG&G PAR potentiostat. The potentiodynamic experiments were performed at 0.5 and 1 mV s^{-1} from −1.7 to −0.8 V, while current densities up to 200 mA cm^{-2} were applied for the efficiency determinations. The experimental results were corrected for the *IR* drop. The solution resistances between the surface of the alloy and the tip of the Luggin capillary were determined by means of impedance mesaurements at high frequencies. At 25 and 50 °C such solution resistances were found to be about 1.0 and 0.6 Ω, respectively.

The corrosion rates (v_{cor}) were determined by weight loss measurements. The electrodes, prepared as indicated above, were weighed and immersed in the test electrolyte for 2–5 h (depending on the electrolyte conditions). Afterwards, the specimens were rapidly removed from the solution, thoroughly washed with Millipore Milli Q water, dried and weighed.

The anode efficiency (*AE*) was determined also by weight loss in galvanostatic experiments at 50, 75, 100 and 125 mA cm^{-2} for 2–4 h. The experimental procedure was the same

as in the corrosion rate measurements. The anode efficiency (%) was calculated as:

$$AE = 100(W_t/W_o) \quad (1)$$

where W_t is the theoretical weight loss corresponding to the impressed current and W_o, the observed weight loss. The weight loss measurements for corrosion rate and anode efficiency determinations were repeated at least three times in order to test the reproducibility of the technique and to obtain reliable results.

2.3. Microscopic examination

The surface of the samples was examined before and after the electrochemical experiments in a 405M Axiovert metallographic microscope and in a JEOL-JSM 840 SEM furnished with an EDX (Link Systems) microanalysis. The microstructure of the Al–2.7%Mg–0.19%Cr–0.04%Mn alloy was studied by means of the modified Poulton's reagent [29] and also using a Philips CM30 TEM, after being cut and submitted to a conventional twin jet electropolishing.

The samples to be observed under SEM were removed from the solution immediately after the experiment, thoroughly rinsed in Millipore Milli Q water and also in ethanol or benzene, dried and stored under high vacuum.

3. Results

The SEM, TEM and metallographic microscopic observations of the specularly polished Al–2.7%Mg–0.19%Cr–0.04%Mn alloy showed elongated grains (because of the rolling process) and the presence of a quite uniform dispersion of micron-sized particles (particles of about 1 μm shown in the central part of Fig. 1). The EDX microanalysis in the TEM conditions demonstrated a uniform Mg distribution, in agreement with the solubility of Mg in Al, except in such micron-sized particles. It should be noted that the Mg content of the alloy was evidenced by a shoulder in the lowest energies of the Al (gaussian) peak. However, the Mg content was sufficient to show by EDX microanalysis that the relative quantity of this element was constant through the sample, i.e., in the Al matrix and in the grain boundaries. In addition, Cr was found to be uniformly dispersed through the sample and Fe was detected in a small percentage in the matrix, in agreement with the ability of Mg to dissolve Fe. The EDX microanalysis of the micron-sized particles (see Fig. 1) were, however, very different from those performed in the matrix and in the grain boundaries. The Fe and Si peak counts were highly increased in the spot microanalysis of such precipitates while the Al and Mg peak counts presented a very marked decrease. In particular, the Mg content was insignificant with respect to the Si, Fe and Cr contents. It was then concluded that such precipitates consisted essentially of non-dissolved Fe and Si-rich particles. It should also be noted that Cr was also detected in such precipitates, but in quantities comparable with those found in the matrix and in the grain boundaries.

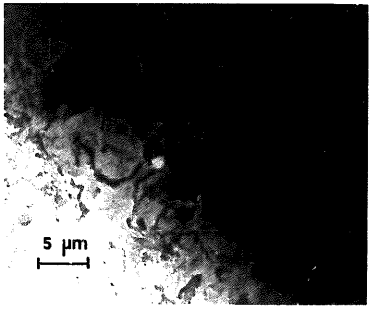

Fig. 1. TEM micrograph of the microstructure of Al–2.7%Mg–0.19%Cr–0.04%Mn alloy.

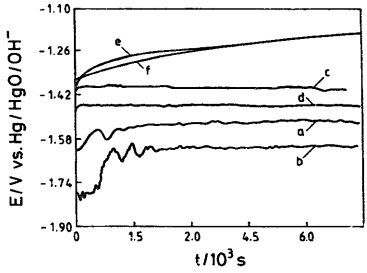

Fig. 2. OCP vs. time of different metals and alloys in 4 M KOH: (a) super-pure Al at 25 °C; (b) super-pure Al at 50 °C; (c) Al–2.7%Mg–0.19%Cr–0.04%Mn at 25 °C; (d) Al–2.7%Mg–0.19%Cr–0.04%Mn at 50 °C; (e) commercial Al at 25 °C, and (f) commercial Al at 50 °C.

The OCP versus time plots for super-pure Al, commercial aluminium and Al–2.7%Mg–0.19%Cr–0.04%Mn in air-saturated and vigorously stirred 4 M KOH solutions at 25 and 50 °C are shown in Fig. 2. The OCPs initially changed to more positive values but, finally, stationary values were approached (curves (a)–(f)). For super-pure Al and Al–2.7%Mg–0.19%Cr–0.04%Mn, the OCPs were about 100 mV more negative at 50 °C than at 25 °C. Commercial Al did not show a stationary corrosion potential even after a 2-h test (curves (e) and (f)), although the potential changed slowly with time after the first hour of immersion. During the first hour at 25 °C, the potential increased from −1.35 to −1.22 V and at 50 °C, from −1.38 to −1.23 V. Finally, OCP at 50 °C approached OCP at 25 °C. The stationary OCPs of Al–2.7%Mg–0.19%Cr–0.04%Mn were more negative (see Fig. 2 and Tables 1 and 2) and it is interesting to note that the stability of the OCPs was attained after about 1 min, both at 25 and 50 °C, while the OCPs corresponding to super-pure Al were quasi-stationary only after 20 min of immersion at 25 °C and after 40 min at 50 °C.

Table 1
Initial OCP (E_0/mV), stationary OCP (E_{st}/mV), potential of zero current of the potentiodynamic polarizations ($E_{I=0}$/mV) and corrosion rate (v_{cor}/mg cm^{-2} min^{-1}) of the Al–2.7%Mg–0.19%Cr–0.04%Mn alloy in 4 M KOH with different additives, at 25 °C

Electrolyte	E_0	E_{st}	$E_{I=0}$	v_{cor}
a = 4 M KOH	−1409	−1392	−1417	0.452
b = a + 10^{-3} M K_2MnO_4	−1443	−1395	−1498	0.458
c = b + 10^{-2} M $NaBiO_3$	−1468	−1438	−1471	0.896
d = c + 10^{-2} M $NaVO_3$	−1472	−1420	−1477	0.431
e = d + 10^{-2} M $NaMoO_4$	−1416	−1414	−1385	0.550
b1 = b + 0.05% Al	−1488	−1481	−1471	0.364
c1 = c + 0.05% Al	−1600	−1585	−1479	0.287
d1 = d + 0.05% Al	−1466	−1436	−1444	0.477
e1 = e + 0.05% Al	−1425	−1422	−1379	0.640

Table 2
Initial OCP (E_0/mV), stationary OCP (E_{st}/mV), potential of zero current of the potentiodynamic polarizations ($E_{I=0}$/mV) and corrosion rate (v_{cor}/mg cm^{-2} min^{-1}) of the Al–2.7%Mg–0.19%Cr–0.04%Mn alloy in 4 M KOH with different additives, at 50 °C

Electrolyte	E_0	E_{st}	$E_{I=0}$	v_{cor}
a = 4 M KOH	−1477	−1470	−1436	1.316
b = a + 10^{-3} M K_2MnO_4	−1429	−1446	−1540	1.200
c = b + 10^{-2} M $NaBiO_3$	−1504	−1503	−1580	1.013
d = c + 10^{-2} M $NaVO_3$	−1600	−1595	−1565	0.680
e = d + 10^{-2} M $NaMoO_4$	−1565	−1519	−1526	1.520
b1 = b + 0.05% Al	−1488	−1441	−1479	1.201
c1 = c + 0.05% Al	−1478	−1442	−1461	0.750
d1 = d + 0.05% Al	−1458	−1446	−1551	0.950
e1 = e + 0.05% Al	−1446	−1428	−1444	0.340
c2 = c1 + 0.05% Zn	−1465	−1466	−1467	1.044

The corrosion rate data in 4 M KOH with K_2MnO_4, $NaBiO_3$, $NaVO_3$, Na_2MoO_4, Al_2O_3, ZnO and combinations thereof at 25 and 50 °C are summarized in Tables 1 and 2, respectively. In these Tables, the initial (E_0) and stationary (E_{st}) OCPs are given to investigate the effect of the immersion time. SEM and optical microscopy clearly showed that the corrosion of the test samples were always uniform. The aspect of the alloy surface after its immersion for 2 h in all the solutions investigated showed general corrosion (the surface was very rough), the grain boundaries being not preferentially dissolved. An example is given in Fig. 3(a).

The voltammograms obtained for all the electrolyte compositions were of the type shown in Fig. 4. The anodic current was shown to approach a constant limiting value. These anodic limiting currents depended on the temperature, being about 125 and 500 mA cm^{-2} at 25 and 50 °C, respectively, for all the working solutions employed. The corresponding OCPs and the potentials of zero current, $E_{I=0}$, are also listed in Tables 1 and 2.

The galvanostatic polarization curves are of the type shown in Fig. 5. Curve (a) presents a constant potential value and the most part of the galvanostatic curves were of this type. Curve (b) presented a smooth and small potential increase up to a stationary value. Note that curve (c) was obtained

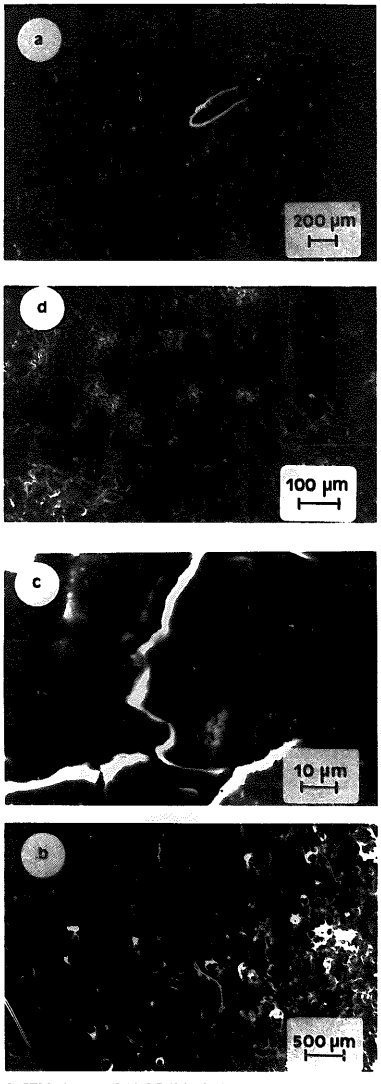

Fig. 3. SEM pictures of Al–2.7%Mg–0.19%Cr–0.04%Mn after different electrochemical treatments: (a) 2 h at OCP in 4 M KOH at 50 °C; (b) 100 mA cm^{-2} at 50 °C in solution c1; (c) 200 mA cm^{-2} at 25 °C in solution c (the oxide cracks are due to the dehydration of the oxide in the process of the sample preparation to be observed under the SEM), and (d) 200 mA cm^{-2} at 50 °C in solution c2, see Table 1.

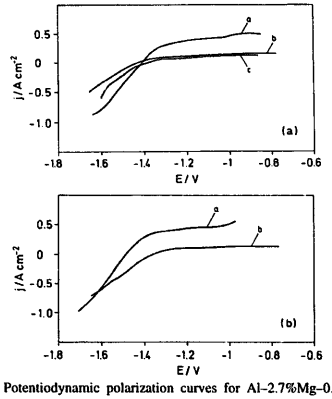

Fig. 4. Potentiodynamic polarization curves for Al–2.7%Mg–0.19%Cr–0.04%Mn in different solutions at different temperatures and 1 mV s^{-1}. (a) 4 M KOH at 25 °C (curve (a)), solution e1 at 25 °C (curve (b)), 4 M KOH at 50 °C (curve (c)). (b) Solution b at 25 °C (curve (d)), and solution c2 at 50 °C (curve (e)); see also Table 1.

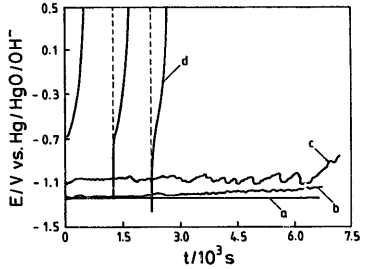

Fig. 5. Typical galvanostatic curves for Al–2.7%Mg–0.19%Cr–0.04%Mn alloy in different solutions at different temperatures and current densities: (a) solution d at 25 °C and 100 mA cm^{-2}; (b) solution c at 25 °C and 100 mA cm^{-2}; (c) solution d1, unstirred, at 25 °C and 100 mA cm^{-2}, and (d) solution d1 at 25 °C and 200 mA cm^{-2}, see Table 1.

without stirring (and compared with the E_{st} potential given in Table 1). When the current density was sufficiently high, that is over the limiting value of the voltammograms, the potential presented a rapid increase followed by a rapid decay (curve (d)), this being repeated several times or even only a continuous increase in potential leading to passivation. As shown in Fig. 3(c), the anode surface was covered with an oxide film after the galvanostatic experimcnt of type (d). The examples shown in Fig. 3(b) and (d) show a quite uniform dissolution of the alloy under galvanostatic experiments for current densities lower than the limiting values. The anode efficiencies were obtained at current densities between 50 and 125 mA cm^{-2} because of the anode passivation over 125 mA cm^{-2} at 25 °C. The corresponding values at 25 and 50 °C are

Table 3
Anode efficiency of Al–2.7%Mg–0.19%Cr–0.04%Mn alloy in stirred 4 M KOH solutions with different additives, at 25 °C and different current densities, j

Electrolyte	Anode efficiency (%)	
	50	100
a = 4 M KOH	35.2	78.20
b = a + 10^{-3} M K_2MnO_4	24.2	81.1
c = b + 10^{-2} M $NaBiO_3$	30.1	86.2
d = c + 10^{-2} M $NaVO_3$	24.4	78.1
e = d + 10^{-2} M $NaMoO_4$	61.0	90.6
b1 = b + 0.05% Al	43.7	83.9
c1 = c + 0.05% Al	66.6	95.2
d1 = d + 0.05% Al	52.4	92.6
e1 = e + 0.05% Al	37.0	84.2

Table 4
Anode efficiency of Al–2.7%Mg–0.19%Cr–0.04%Mn alloy in stirred 4 M KOH solutions with different additives, at 50 °C and different current densities, j

Electrolyte	Anode efficiency (%)			
	50	75	100	125
a = 4 M KOH	17.4	26.0	31.4	43.3
b = a + 10^{-3} M K_2MnO_4	18.8	39.2	41.3	36.6
c = b + 10^{-2} M $NaBiO_3$	17.1	17.2	27.3	38.7
d = c + 10^{-2} M $NaVO_3$	12.2	23.1	36.0	37.7
e = d + 10^{-2} M $NaMoO_4$	21.1	23.6	22.5	42.3
b1 = b + 0.05% Al	37.8	25.8	38.3	36.3
c1 = c + 0.05 %Al	15.3	22.8	45.8	61.6
d1 = d + 0.05% Al	15.6	32.0	43.5	59.8
e1 = e + 0.05% Al	47.4	36.4	50.5	46.6
c2 = c1 + 0.05% Zn	30.4	53.6	30.0	34.0

shown in Tables 3 and 4 and the stationary potentials at different current densities, also at 25 and 50°C, in Table 5.

4. Discussion

The microstructural analysis of Al–2.7%Mg–0.19%Cr–0.04%Mn did not show any (Al, Mg) precipitates in the grains, as expected for alloys having up to 4% Mg [30,31]. The SEM observations of this alloy after several hours of exposure to the investigated alkaline media showed the existence of a general dissolution alhough the anode surface was quite rough (Fig. 3(a)). The absence of localized penetration of the anodes in bateries is necessary to avoid premature disintegration.

As shown in Fig. 2, the OCPs of Al–2.7%Mg–0.19%Cr–0.04%Mn in 4 M KOH were, both at 25 and 50 °C, more positive than that of super-pure Al but more negative than that of commercial Al. The stationary potentials given in Tables 1 and 2 are in the range − 1.4 to − 1.6 V, these being considered as good anode potentials for battery applications [6,17,20,22]. In addition, these OCPs were constant at least for 2 h, which was the time of the experiment (see Fig. 2).

Table 5
Stationary potentials at different current densities (j) of Al–2.7%Mg–0.19%Cr–0.04%Mn alloy in 4 M KOH, in mV vs. Hg/HgO/KOH (4 M), with different additives, at 25 and 50 °C

Electrolyte	j at 25 °C (mA cm^{-2})		j at 50 °C (mA cm^{-2})		
	50	100	50	100	125
a = 4 M KOH	−1426	−1360	−1470	−1418	−1337
b = a + 10^{-3} M K_2MnO_4	−1166	−1109	−1481	−1495	−1478
c = b + 10^{-2} M $NaBiO_3$	−1329	−1287	−1395	−1379	−1228
d = c + 10^{-2} M $NaVO_3$	−1409	−1352	−1483	−1495	−1420
e = d + 10^{-2} M $NaMoO_4$	−1350	−1184	−1447	−1456	−1408
b1 = b + 0.05%Al	−1355	−1120	−1452	−1317	−1318
c1 = c + 0.05%Al	−1370	−1220	−1420	−140	−1375
d1 = d + 0.05%Al	−1431	−1297	−1505	−1374	−1318
e1 = e + 0.05%Al	−1371	−1240	−1394	−1340	−1240
c2 = c1 + 0.05%Zn			−1339	−1345	−1336

Note also that this alloy rapidly reached the stationary OCP, in the presence and in the absence of the inhibitors, while much greater times are needed for super-pure Al and commercial Al.

In contrast with the good anode potentials, the corrosion rates in stand-by conditions are high (Tables 1 and 2), in particular at 50 °C. Such high corrosion rates appear to be related with an excess of Mg [6,20]. The lowest corrosion rate was one order of magnitude greater than that of alloy BDW [9,26] at 50 °C in 4 M KOH (5 mA cm^{-2}, that is 0.028 mg cm^{-2} min^{-1}). However, they are of the same order of magnitude as for super-pure Al also in inhibited 4 M KOH, which were in the range 0.1–1.6 mg cm^{-2} min^{-1} (19–290 mA cm^{-2}). However, it is generally accepted that aluminium anodes in alkaline aluminium batteries must not be in contact with the electrolyte when the battery does not operate [6,20]. The anode would always be destroyed after a sufficient period of exposition without power generation.

The corrosion rates when the current flows through the anode must also be analysed in detail. As described in the results section, the anodic current increases after $E_{I=0}$ but the j-E slope decreases, the total current tending to a constant limiting value (Fig. 4). Such a tendency is due to a surface oxide film, in agreement with the transpassive mode of the anode dissolution of Al in these conditions of potential and KOH concentration [32]. Such an oxide presents a small resistance and permits the anode dissolution through it. The electrolyte composition also allows the oxide dissolution. The interesting situation in batteries is a constant and high j-E slope, what means a small resistance and the continuous anode oxidation through a film which presents a high conductivity. For this reason, the troublesome result in the voltammograms of Fig. 4(a) and (b) is the tendency to a constant current region of about 125 and 500 mA cm^{-2} at 25 and 50 °C, respectively, what means that the energy production cannot exceed a limiting value.

The galvanostatic curves shown in Fig. 5 are consistent with the voltammograms of Al–2.7%Mg–0.19%Cr–0.04%Mn. As shown in Figs. 3(c) and 5 (curve (d)), an oxide film which passivates the anode is formed at sufficiently high current densities, e.g. currents over the limiting values. This limits the interest of this alloy, because typical current densities in batteries for vehicles are 100–250 mA cm^{-2} and in the reserve batteries, 50–150 mA cm^{-2} and a strict control of the temperature would be necessary.

When comparing the curves (b) and (c) in Fig. 5, it appears that for current densities near the limiting value at the corresponding temperature, the anode becomes partially protected when the layer on the anode surface is not removed by stirring (curve (c)) and a passivating oxide film may further develop. In contrast, stirring avoids the accumulation of aluminate in the electrolyte layer on the anode and dissolves the oxide which can be formed, the anodic current producing a porous or gel-like protective oxide layer having a small resistance. Stationary potentials result from these latter conditions of constant current (curves (a) and (b)). The anode efficiencies are then only meaningful for galvanostatic curves of the types (a) and (b) of Fig. 5, conditions which permit the anode dissolution for a long time (at least 2 h, see Fig. 5, curves (a) and (b)). Accordingly, the anode efficiencies are only meaningful for galvanostatic curves of the types (a) and (b) of Fig. 5. When comparing the galvanostatic curves at 25 and 50 °C, it is found that greater anodic current densities can be achieved at the latter temperature without passivation. This is explained by an increase in the solubility of the film at 50 °C.

As shown in Tables 3 and 4, the anode efficiencies generally increase with current density and at 25 °C, they are higher than at 50 °C, this being in agreement with the formation of a film which is less protective when the temperature increases and the current density decreases. It is also shown that the anode efficiencies continue to be very low and only present reasonable values for currrents densities which approach the limiting values. This indicates that Al–2.7%Mg–0.19%Cr–0.04%Mn with 0.27% Fe and 0.14% Si would be useful in aluminium batteries with inhibited alkaline solutions only in a limited range of current densities at a given temperature and restricted hydrodynamic conditions (for the oxide dissolution). The presence of Cr in the alloy does not lead then to the expected values of the anode efficiencies of the Al–Mg

alloys in the presence of Fe and Si. On the other hand, the presence of Cr may be responsible for the anode passivation at current densities which would be useful for vehicle applications, in the absence of a strict control of the temperature. The behaviour of Cr appear then to be similar to that of Mn, because an excess of the alloying element may lead to the anode passivation. This suggests that better behaviour should be obtained for lower Cr contents and in the absence of Fe and Si in the alloy.

5. Conclusions

The stationary OCPs of Al–2.7%Mg–0.19%Cr–0.04%Mn, containing 0.27% Fe and 0.14% Si, in 4 M KOH inhibited by the addition of K_2MnO_4 and combinations of $NaVO_3$, $NaBiO_3$, $NaMoO_4$, ZnO and Al_2O_3 were in the range from -1.4 to -1.6 V versus Hg/HgO/OH^- both, at 25 and 50 °C. Such stationary values were rapidly achieved and were good anode potentials for application in batteries. However, the corrosion rates were too high. The lowest open-circuit corrosion rates at 25 °C were found for 4 M KOH containing K_2MnO_4, $NaBiO_3$ and Al_2O_3, while at 50 °C, for 4 M KOH containing K_2MnO_4, $NaBiO_3$, $NaMoO_4$ and Al_2O_3, the corresponding values being 0.29 and 0.34 mg cm^{-2} min^{-1}.

The microscopic observation in stand-by conditions and after anodic polarization showed uniform dissolution of the alloy in 4 M KOH and also in 4 M KOH with different additives. This was correlated with the uniform distribution of Mg in the alloy.

The anodic dissolution was also proved to take place through a partially protective aluminium oxide having small resistance. The anode efficiencies increased with current density. However, they were only sufficiently high, that is over 90%, at current densities approaching the limiting values. Over such limiting values, which depended on the temperature, passivation took place. The possible interest of these alloys for battery applications is then limited to restricted ranges of temperature and current density.

The presence of Cr and Mn in the Al–Mg alloys containing Fe and Si did not lead to the expected increase in the anode efficiencies. Cr behaved similarly to Mn in that an excess of the alloying element could lead to the anode passivation. The results of this first approach to use Al–Mg alloys containing Cr and Mn as anodes in batteries together with previous results in the literature suggest a better performance when using lower contents in Mg and Cr and in the absence of Fe and Si.

Acknowledgements

The authors gratefully acknowledge the contract as 'Professor Visitant' of the Universitad de Barcelona (UB) conceded by the DGU to Dr A.M.M.M. Adam and the 'Serveis Científico-Tècnics de la UB' for the facilities in the SEM and TEM observations and the EDX microanalysis.

References

[1] N.P. Fitzpatrick, F.N. Smith and P.W. Jeffrey, *The Aluminium–Air Battery, Int. Congr. and Exposition, Detroit, MI, USA, 1983*, pp. 63–67.
[2] D.D. Macdonald and C.E. English, *J. Appl. Electrochem., 20* (1990) 405.
[3] J.D. Slisburg, E. Behrin, M.K. Kong and D.J. Wisler, *A Comparative Analysis of Aluminium–Air Battery, Propulsion Systems for Passanger Vehicles*, Livermore, CA, 1990.
[4] J.F. Cooper, Estimates of the cost and energy consumption of Al–air electric vehicles, *Proc. Fall Meet. The Electrochemical Society, Hollywood, FL, USA, 1980.*
[5] M. Ritschel and W. Vieltich, *Electrochim. Acta, 24* (1979) 885.
[6] J.A. Hunter, G.M. Scamans and W.B. O'Callaghan, *US Patent No. 4 942 100* (1990).
[7] S. Zaromb, *US Patent No. 3 513 031* (1970).
[8] W.A. Bryant and E.S. Buzzelli, A comparative study of metal–air batteries for electric vehicle propulsion, *Proc. 14th Conf.*, 1979, pp. 651–653.
[9] M. Makran, *Comp. Rend., 245* (1957) 1060.
[10] A.N. Mukheryi, S. Lider and V.S. Alkekar, *Br. Corros. J., 3* (1975) 155.
[11] M. Kato and K. Tanaka, *Kagaku Zaschi, 68* (1964) 166.
[12] T.A. Kravchenko, A.Ya. Shatalov and E.K. Yanchuk, *Khlim. Tekhnol., 7* (1964) 56.
[13] C. Rama, Dextrin as an inhibitor for the corrosion of aluminium in acid and alkaline solution, in *Int. Symp. Anticorrosion Protection, Bratislava, Slovenia, 1962*, p. 1.
[14] M. Krishnan and N. Subramanyan, *Corros. Sci., 11* (1977) 893.
[15] J.D. Talati and N.H. Joshi, *Werkst. Korros., 7* (1978) 461.
[16] L.D. Shrylev, E.C. Markina and N.H. Purich, *Zasch. Met., 4* (1991) 685.
[17] A.R. Despic, D.M. Drazic, M.M. Purenovic and N. Cicovoc, *J. Appl. Electrochem., 6* (1976) 527.
[18] A.R. Despic, D.M. Drazic, S.K. Zecevic and R.T. Atanasoski, *Electrochim. Acta, 26* (1981) 173.
[19] D.D. Macdonald, S. Real and M. Urquidi-Macdonald, *J. Electrochem. Soc., 135* (1988) 2397.
[20] J.A. Hunter, G.M. Scamans, W.B. O'Callaghan and P.A. Wycliffe, *US Patent No. 5 004 654* (1991).
[21] K.B. Sarangapani, V. Balaramachandran, V. Kapali, S. Venkatakrishna, M.G. Podtar and K.S. Rajagopalan, *J. Appl. Electrochem., 14* (1984) 480.
[22] A. Sheik, M. Ganesan, M. Anbukulandainathan, K.B. Sarangapani, V. Balaramachandran, V. Kapali and S. Venkatakrishna, *J. Power Sources*, 27 (1987) 243.
[23] T. Valand, The effect of impurities and low level alloying elements on aluminium for use in Al/air cells, in *Proc. 160th Electrochemical Society Meet., Oct. 1981.*
[24] L.G.S. Rosilda, M. Ganesan, M.A. Kulandainathan and V. Kapali, *J. Power Sources, 50* (1994) 321.
[25] L.F. Mondolfo, *Metall. Rev., 16* (1971) 95.
[26] M. Zamin, *Corrosion (Houston), 37* (1981) 627.
[27] M.J. Pryor, *US Patent No. 3 186 836* (1965).
[28] K.A. Jensen and V. Klemn, *Z. Anorg. Allg. Chem., 237* (1938) 47.
[29] American Society of Metals, Metallography and microstructures, in *Metals Handbook*, Vol. 9, ASM, Metals Park, OH, 9th edn., 1985, pp. 352–354.
[30] F. King, *Aluminium and its Alloys*, Ellis Horwood, Chichester, UK, 1987, p. 95; p. 170.
[31] I.J. Polmear, *Light Metals, Metallurgy of the Light Metals*, Edward Arnold, London, 2nd. edn., 1984, p. 161.
[32] D.D. Macdonald, S. Real, S.I. Smedley and M. Urquidi-Macdonald, *J. Electrochem. Soc., 135* (1988) 2410.